Title

Effect of graphene-based nanomaterials on corneal wound healing in vitro

Authors

Fukuto, Atsuhiko

Kang, Jennifer

Gates, Brooke L

et al.

Publication Date

2023-04-01

DOI

10.1016/j.exer.2023.109419

Peer reviewed

HHS Public Access

Author manuscript

Exp Eye Res. Author manuscript; available in PMC 2023 April 26.

Published in final edited form as:

Exp Eye Res. 2023 April ; 229: 109419. doi:10.1016/j.exer.2023.109419.

Effect of graphene-based nanomaterials on corneal wound healing *in vitro*

Atsuhiko Fukuto[a,b,1], **Jennifer Kang**[a,1], **Brooke L. Gates**[a], **Kimberley Sannajust**[a], **Kent E. Pinkerton**[c,e], **Laura S. Van Winkle**[c,e], **Yoshiaki Kiuchi**[b], **Brian C. Leonard**[a], **Sara M. Thomasy**[a,d,*]

[a]Department of Surgical and Radiological Sciences, School of Veterinary Medicine, University of California-Davis, Davis, CA, 95616, USA

[b]Department of Ophthalmology and Visual Sciences, Graduate School of Biomedical and Health Sciences, Hiroshima University, Minami-ku, Kasumi 1-2-3, Hiroshima, 734-8551, Japan

[c]Center for Health and the Environment, University of California-Davis, Davis, CA, 95616, USA

[d]Department of Ophthalmology & Vision Science, School of Medicine, University of California-Davis, Davis, CA, 95616, USA

[e]Department of Anatomy, Physiology and Cell Biology, School of Veterinary Medicine, University of California-Davis, Davis, CA, 95616, USA

Abstract

Graphene-based nanomaterials (GBNs) are widely used due to their chemical and physical properties for multiple commercial and environmental applications. From an occupational health perspective, there is concern regarding the effects of inhalation on the respiratory system, and many studies have been conducted to study inhalation impacts on lung. Similar to the respiratory system, the eyes may also be exposed to GBNs and thus impacted. In this study, immortalized human corneal epithelial (hTCEpi) cells and rabbit corneal fibroblasts (RCFs) were used to investigate the toxicity of eight types of GBN: graphene oxide (GO; 400 nm), GO (1 μm), partially reduced graphene oxide (PRGO; 400 nm), reduced graphene oxide (RGO; 400 nm), RGO (2 μm), graphene (110 nm), graphene (140 nm), and graphene (1 μm). We next examined the effects of these GBNs on hTCEpi cell migration. We also determined whether the expression of α-smooth muscle actin (αSMA), a myofibroblast marker, is altered by the GBNs using RCFs. We found that RGO (400 nm) and RGO (2 μm) were highly toxic to hTCEPi cells and RCFs meanwhile, PRGO (400 nm) was toxic only to hTCEpi cells. In addition, PRGO (400 nm), RGO (400 nm), and RGO (2 μm) inhibited hTCEpi cell migration and significantly increased αSMA mRNA expression. Further study *in vivo* is required to determine if RGO nanomaterials delay corneal epithelial healing and induce scar formation.

*Corresponding author. Department of Surgical and Radiological Sciences, School of Veterinary Medicine, University of California-Davis, Davis, CA 95616, USA. smthomasy@ucdavis.edu (S.M. Thomasy).

[1]contributed equally, authors listed in alphabetical order.

Declaration of competing interest

The authors declare no conflict of interest.

Keywords

Graphene-based nanomaterials; Corneal wound healing; Keratocyte-fibroblast-myofibroblast transformation

1. Introduction

There has been significant interest in derivatives of graphene-based nanomaterials (GBNs), particularly graphene oxide (GO), given their electrochemical and physicochemical properties (Lee et al., 2019). Specifically, their functionalization allows them to be used for an array of applications in biosensing (Yang et al., 2013), drug delivery (Zahin et al., 2020), and antimicrobial materials (Giulio et al., 2018; Mohammed et al., 2020) as well as multiple environmental applications (Perreault et al., 2015). Furthermore, GBNs are being incorporated into contact lenses to increase tear fluid volume (Huang et al., 2021), protect against electromagnetic radiation (Lee et al., 2017), and treat fungal keratitis (Huang et al., 2016). Thus, this increasing use of GBNs raises questions about potential toxicity. Various studies have suggested the dose and time-dependent toxicity of GO. *In vitro* studies on hepatocellular carcinoma cells have demonstrated that penetration of GO through the plasma membrane altered morphology and increased the presence of reactive oxygen species (Lammel et al., 2013). Exposure to GO resulted in oxidative stress in human lung fibroblast cells (Wang et al., 2013), human alveolar basal epithelial cells (Chang et al., 2011), as well as in human skin keratocytes (Pelin et al., 2018).

However, ocular studies are limited, with GO found to be toxic to mouse conjunctiva, while reduced graphene oxide (RGO) was reported to have no harmful effect (An et al., 2018). The mechanism by which GO causes ocular toxicity remains unclear, although the difference in physical characteristics, particularly size, may explain the varying toxicity of GO and RGO (Jiang et al., 2021). Additionally, dose and time-dependent GO toxicity were due to oxidative stress in human corneal epithelial cells and human conjunctiva epithelium cells, while repeated exposure in rats damaged corneal epithelium (Wu et al., 2016).

The eye is in direct contact with its external environment, so it is crucial to understand the effects of GBNs on the eyes. While it is known that ocular exposure to GBNs can cause damage, there is still a lack of understanding of their impact on corneal wound healing. Following an injury to the cornea, cell migration and keratocyte-fibroblast-myofibroblast (KFM) transformation induced by transforming growth factor-β1 (TGF-β1) are critical for proper wound healing (Ljubimov and Saghizadeh, 2015). This study evaluates the *in vitro* toxicity of GO, partially reduced graphene oxide (PRGO), RGO, and graphene nanomaterials on corneal epithelial cells and fibroblasts, epithelial cell migration, and fibroblast-to-myofibroblast differentiation.

2. Materials and methods

2.1. Nanomaterials synthesis and characterization and preparation of suspensions

This study used GBNs generated and characterized by the Engineered Nanomaterials Coordination Core as part of the Nanotechnology Health Implications Research (NHIR)

Consortium at the Harvard T.H. Chan School of Public Health. The 2D GBNs that were assessed in this study include: GO (400 nm), GO (1 μm), PRGO (400 nm), RGO (400 nm), RGO (2 μm), graphene (110 nm), graphene (140 nm), and graphene (1 μm) (Table 1). The GBNs were synthesized using liquid phase exfoliation and/or a derivative of Hummer's method (Duan et al., 2020; Parviz and Strano, 2018). The purity of each of the GBNs was confirmed to be greater than 98% by inductively coupled plasma mass spectrometry (Herner et al., 2006).

The GBNs were resuspended and sonicated with a calibrated sonication system (2510R-MT; Branson Ultrasonic Co., Danbury, CT) as detailed by DeLoid and colleagues (DeLoid et al., 2017) before experimental use. In summary, each NP was placed in a 15 mL conical tube with deionized water added to reach a final concentration of 2 mg/ml. Then the nanosuspensions were vortexed for approximately 30 s at high speed and sonicated for 1 min/ml as described for each material. After sonication, the stock suspensions were vortexed again at high speed for 30 s and diluted to their final concentration with a balanced salt solution (BSS; Alcon, Geneva, Switzerland). After preparation, the diluted suspensions were used immediately, and preparation protocols were repeated every 24 h.

2.2. Cell culture

Primary rabbit corneal fibroblast cells (RCFs) were obtained from enucleated young rabbit eyes (PelFreez, Rogers, AR) after isolated corneas were digested with collagenase and hyaluronidase as previously described (Myrna et al., 2012). The cells were maintained in Dulbecco's Modified Eagle's Medium Low Glucose growth media (HyClone; GE Healthcare Life Sciences, Logan, UT) complemented with 10% fetal bovine serum (Atlanta Biologicals, Lawrence, GA) and 1% penicillin-streptomycin-fungizone (PSF; HyCloneTM 100 × HyClone, Logan, UT) at 37 °C and 5% CO_2. Cells were used between passages 3 to 7.

Human-telomerase reverse transcriptase-immortalized corneal epithelial (hTCEpi) cells were kindly donated by James V Jester, Ph.D. (University of California, Irvine) (Robertson et al., 2005). The cells were cultured at 37 °C, and 5% CO_2 in EpiLife growth media (Life Technologies, Carlsbad, CA) supplemented with 1% EpiLife Defined Growth S (Life Technologies) and 1% PSF (HyCloneTM). Cells were used between passages 40 to 60.

2.3. Cell viability assay

Calcein AM (acetoxymethyl ester) assays were carried out to assess the effects of various graphene nanoparticles on hTCEpi and RCF cell viability. The Calcein-AM Cell Viability Kit (TREVIGEN®, R&D Systems, Inc. Minneapolis, MN) was used to measure cytotoxicity. The RCFs were plated at a density of 5000 cells per well in 100 μl of media or 8000 hTCEpi cells per 100 μl of media in a black-walled 96-well plate. The cells were incubated for 24 h to allow attachment to the bottom of the wells before treatment. Citrate-capped gold nanoparticles (AuNP; 15 nm; 5 μg/ml) and saponin (1 mg/ml) were used as negative and positive controls, respectively. After 24-h incubation with the nanomaterials ranging from 0.05 to 50 μg/ml, the media was replaced with 100 μL of working 1 mM Calcein AM solution in PBS for 30 min at 37 °C under 5% CO_2. Cell fluorescence was read using a microplate reader with a 490 nm excitation filter and a 520 nm emission filter. The viability

test was conducted in triplicates, and absorbance for wells without cells containing the NPs was used as the blank control in both assays. Relative cell viability was calculated by subtracting the blank controls' absorbance values from the treated wells' absorbance values and multiplying by 100 to give the value as percent viabilities. These values were normalized to the vehicle control.

2.4. RNA extraction and quantitative real-time PCR

RCFs were seeded at 1.5×10^5 per 2 ml of media in 6-well plates. After allowing cells to attach for 24 h, the media was aspirated and replaced with culture media containing graphene NPs or distilled water (vehicle control) in the presence or absence of 10 ng/ml of TGF-β1. RNA was extracted 24 h after treatment using the GeneJET RNA Purification Kit (Thermo Fisher Scientific, Waltham, MA), following the manufacturer's protocol. A NanoDrop ND-1000 spectrophotometer (Thermo Fisher Scientific) was used to quantify the RNA by measuring the absorbance at 260 nm. Quantitative real-time PCR (qPCR) was performed with SensiFAST Probe Hi-ROX One-Step kit (Bioline, Taunton, MA) using rabbit-specific aptamers for α-smooth muscle actin (αSMA; *ACTA2*, Oc03399251_m1; Thermo Fisher Scientific) and glyceraldehyde 3-phosphate dehydrogenase (*GAPDH*, Oc03823402_g1; Thermo Fisher Scientific), which served as a housekeeping gene. The results were expressed as $2^{-\mathbf{\Delta\Delta CT}}$ with *GAPDH* used as the reference. The total reaction volume was 10 μl per reaction, and each reaction was performed in triplicates; experiments were run at least three times. Gene expression was normalized relative to mRNA expression of cells treated with the vehicle control and the absence of TGF-β1.

2.5. Epithelial cell migration assay

In vitro cell migration of hTCEpi cells was measured using the Oris™ 96-well cell migration assay kit (Platypus Technologies, Madison, WI), following the manufacturer's instructions. In summary, 2×10^4 hTCEpis per 100 μl of media were seeded in black-walled 96-well plates containing the cell stoppers in the middle of each well. Once a monolayer of cells was formed, the cell stoppers were carefully removed, and the cells were treated with various GBNs at concentrations selected based on cell viability results. Cytochalasin D (1 μg/ml) was used as a positive control. The cells were incubated for 24 h to allow migration into the detection zone. Then they were fixed for 30 min with 4% paraformaldehyde in PBS. The cells were washed with Dulbecco's Phosphate Buffered Saline, and their nuclei were stained with 4′,6-diamidino-2-phenylindole (DAPI; BioGenex, San Ramon, CA) 1:20,000 in PBS for 15 min at room temperature. Immediately after staining, the cells were imaged with a fluorescence microscope with a 4 × objective (BZ-×800; Keyence Co., Osaka, Japan). The area of the cell-free region was measured using ImageJ analysis software (ver 1.52k; National Institute of Health, Bethesda, MD), and the relative cell migration was calculated for the media control.

2.6. Statistical analysis

Cell viability and migration data were analyzed by one-way ANOVA followed by Dunnett's multiple comparisons test. Real-time PCR data were analyzed by one-way ANOVA followed by Tukey's multiple comparisons test. All statistical analyses were performed using

GraphPad Prism software version 9.4.0 for macOS (GraphPad Software LLC., San Diego, CA). A p-value of <0.05 was considered statistically significant.

3. Results

3.1. Cytotoxicity of GBNs to hTCEpi cells

The cell viability of the hTCEpi cells was evaluated after 24-h exposure to various GBNs using the Calcein AM assay. Of the eight nanomaterials tested, PRGO (400 nm), RGO (400 nm), RGO (2 μm), and graphene (110 nm) were significantly cytotoxic to hTCEpi cells. In particular, RGO (400 nm) showed substantial toxicity at concentrations >12.5 μg/ml. The remaining four nanomaterials — GO (400 nm), GO (1 μm), graphene (140 nm), and graphene (1 μm) — showed no significant toxicity to hTCEpi cells at concentrations as high as 50 μg/ml (Fig. 1).

3.2. The hTCEpi cell migration after exposure to GBNs

We evaluated the effects of eight GBNs on cell migration using a round wound healing assay. Among the GBNs, GO (400 nm), GO (1 μm), PRGO (400 nm), RGO (400 nm), and RGO (2 μm) significantly inhibited cell migration even at low concentrations of 2.5 and 5 μg/ml. Graphene (110 nm) and graphene (140 nm) significantly inhibited cell migration at concentrations >25 μg/ml and 50 μg/ml, respectively. Graphene (1 μm) did not affect cell migration even at the highest tested concentration of 50 μg/ml (Fig. 2).

3.3. Cytotoxicity of GBNs to RCFs

Cell viability of RCFs after 24 h of exposure to various types of GBN was evaluated using the Calcein AM assay (Fig. 3). Only RGO (400 nm) and RGO (2 μm) were significantly cytotoxic to RCF at concentrations >12.5 μg/ml. The remaining six GBNs were not cytotoxic even at the maximum tested concentration of 50 μg/ml.

3.4. TGF-β1-induced αSMA mRNA expression of RCFs after exposure to GBNs

We studied the effects of the eight GBNs on αSMA mRNA expression using quantitative real-time PCR (Fig. 4). PRGO (400 nm), RGO (400 nm), and RGO (2 μm) significantly increased αSMA mRNA expression in the presence of TGF-β1. The remaining five GBNs had no significant effect on αSMA mRNA expression.

4. Discussion

Clinical application of GBNs is underway in the field of ophthalmology. For example, GBN-containing contact lenses have been developed with the added value of treating dry eye syndrome (Huang et al., 2021) and fungal keratitis (Huang et al., 2016), and shielding electromagnetic waves (Lee et al., 2017). Since contact lenses are in contact with the cornea for long periods of time, it is significant to evaluate the impact of GBNs on the cornea. This study described the *in vitro* cytotoxic effects of various GBNs on corneal epithelial cells and stromal fibroblasts. The PRGO (400 nm), RGO (400 nm), and RGO (2 μm) were all cytotoxic to hTCEpi cells even at low concentrations. By contrast, exposure of hTCEpi cells to GO (400 nm) and GO (1 μm) at concentrations of 50 μg/ml resulted in only a

slight, statistically insignificant decrease in cell viability of approximately 80%. These cell viabilities were similar to those obtained when mouse corneal epithelial cells were exposed to GO at 50 μg/ml (An et al., 2018). In contrast, Wu et al. reported that GO is toxic to human corneal epithelial cells, with cell viability reduced to 40% when exposed to concentrations of 50 μg/ml (Wu et al., 2016). This difference may be attributed to the GO size; Wu et al. used 120 nm GO, smaller than the GO sizes used in this study (400 nm and 1 μm). Generally, the smaller the size of a GO, the more toxic it is (Seabra et al., 2014). The fact that RGO (400 nm) was more toxic than RGO (2 μm) in this study may also be due to the size difference. PRGO (400 nm) and RGO (400 nm) were comparable in size, but RGO (400 nm) was more toxic to hTCEpi cells. This result is also consistent with a report that RGO became more harmful to human retinal pigment epithelium as the degree of reduction increased (Ou et al., 2021). None of the three graphene nanomaterials tested in this study was toxic at concentrations below 25 μg/ml. This difference in toxicity between graphene and GO versus RGO may be explained by hydrophilicity and functional groups. Graphene and RGO are hydrophobic and therefore have high affinity to cell membranes. GO and RGO have many carbonyl groups, which are considered toxic functional groups (Chng and Pumera, 2013). Thus, the hydrophobicity of RGO combined with its carbonyl groups may have disrupted the cell membrane.

We have previously reported the toxicity of various metal oxide nanomaterials on corneal epithelial cells and fibroblasts. Previous studies demonstrated that most metal oxide nanomaterials displayed similar toxicity to hTCEpi cells and RCFs (Fukuto et al., 2021; Kim et al., 2020). In the present study, RGO (400 nm) and RGO (2 μm) were also toxic to both cell types. The two RGO nanomaterials were toxic to hTCEpi at 5 μg/ml and RCF at 12.5 μg/ml, comparable to the toxicity of V_2O_5 nanoflakes (Fukuto et al., 2021; Kim et al., 2020). Limited publications evaluate the toxicity of graphene nanomaterials on human epithelial cells and fibroblasts, with no or low toxicity at concentrations lower than 10 μg/ml (Liao et al., 2011; Nasirzadeh et al., 2019; Park et al., 2015). Similarly, the graphene nanomaterials used in this study were not toxic to hTCEpi cells or RCF at concentrations below 12.5 μg/ml.

Epithelial cell migration is a crucial property of corneal wound healing. All GO forms (GO, PRGO, and RGO) tested in this study decreased epithelial cell migration in a dose-dependent matter. GO nanosheets inhibited cell migration of human alveolar basal epithelial (A549) cells by interfering with the structure of the actin filaments (Tian et al., 2017). RGO nanomaterials increased cell migration of A549 cells at concentrations lower than 10 μg/ml, while migration was inhibited at 20 μg/ml (Liao et al., 2018). The difference in the effect of low concentrations of RGO on cell migration between A549 and hTCEpi cells suggests that tolerance to RGO may vary from organ to organ.

KFM transformation also plays an essential role in corneal wound healing. When the cornea is injured *in vivo*, keratocytes differentiate into fibroblasts and migrate to the injury site (Fini and Stramer, 2005). As wound healing progresses, fibroblasts differentiate into αSMA-positive myofibroblasts (Jester et al., 1995). This differentiation is promoted by TGF-β1 secreted by corneal epithelial cells (Jester et al., 1999). If this reaction is excessive, the corneal parenchyma becomes fibrotic, resulting in corneal opacification and impaired visual

function (Wilson, 2020). Similarly, GO and RGO nanomaterials induce lung fibrosis via epithelial-mesenchymal transition (Kan et al., 2022; Liao et al., 2018). In the current study, PRGO and RGO nanomaterials significantly increased αSMA gene expression, while GO and graphene nanomaterials did not show significant changes.

A limitation of this study is that there is an upper limit to the concentration of GBNs that can be tested in the cell viability assay. According to the U.S. Environmental Protection Agency's acute toxicity classification, a chemical is considered essentially nontoxic if its median lethal concentration (LC50) exceeds 100 μg/ml (Hemmer et al., 2011). Therefore, the maximum concentration for cell viability assays should ideally exceed 100 μg/ml. As can be seen in Tables 1 and 8 GBNs are available in concentrations ranging from 310 μg/ml to 500 μg/ml. The maximum concentration of GBNs used in the cell viability assay was set at 50 μg/ml to minimize the effects of dispersants on cells.

It is important to consider the effects of metal/metal oxide NPs on corneal epithelial and stromal wound healing since *in vitro* and *in vivo* results are always congruent. For example, zinc oxide, vanadium pent-oxide, and silver silica NPs inhibited corneal epithelial cell migration *in vitro*, but only zinc oxide NPs delayed corneal epithelial wound closure *in vivo* (Kim et al., 2020, 2021). Iron oxide NPs increased αSMA mRNA expression in corneal fibroblasts *in vitro* but did not alter corneal stromal haze formation *in vivo* (Fukuto et al., 2021). In the present study, we investigated the effect of GBNs on corneal epithelial and stromal wound healing *in vitro*, but whether the same phenomenon occurs *in vivo* warrants further investigation in animal models.

5. Conclusion

GBNs vary in toxicity to corneal epithelial cells and fibroblasts depending on their size and degree of redox. We show that GO, PRGO, and RGO nanomaterials significantly inhibit the migration of corneal epithelial cells even at low concentrations, suggesting that they prolong corneal epithelial defects. Furthermore, PRGO and RGO nanomaterials significantly induced KFM transformation, indicating that they may leave scars after corneal wound healing.

Funding

These studies were funded by grants from the National Institutes of Health - NIEHS U01 ES027288, NEI R01 EY019970, NEI K08 EY028199, and NEI P30 EY012576 and conducted as part of a Nanotechnology Health Implications Research (NHIR) Consortium with the Coordination Core established at the Harvard University T.H. Chan School of Public Health. The NIEHS Nanosafety Center provided all GBNs (U24 ES026946).

Data availability

Data will be made available on request.

References

An W, Zhang Y, Zhang X, Li K, Kang Y, Akhtar S, Sha X, Gao L, 2018. Ocular toxicity of reduced graphene oxide or graphene oxide exposure in mouse eyes. Exp. Eye Res 174, 59–69. [PubMed: 29803558]

Chang Y, Yang ST, Liu JH, Dong E, Wang Y, Cao A, Liu Y, Wang H, 2011. In vitro toxicity evaluation of graphene oxide on A549 cells. Toxicol. Lett 200, 201–210. [PubMed: 21130147]

Chng ELK, Pumera M, 2013. The toxicity of graphene oxides: dependence on the oxidative methods used. Chem. Eur J 19, 8227–8235. [PubMed: 23630053]

DeLoid GM, Cohen JM, Pyrgiotakis G, Demokritou P, 2017. Preparation, characterization, and in vitro dosimetry of dispersed, engineered nanomaterials. Nat. Protoc 12, 355–371. [PubMed: 28102836]

Duan Y, Coreas R, Liu Y, Bitounis D, Zhang Z, Parviz D, Strano M, Demokritou P, Zhong W, 2020. Prediction of protein corona on nanomaterials by machine learning using novel descriptors. NanoImpact 17.

Fini ME, Stramer BM, 2005. How the cornea heals: cornea-specific repair mechanisms affecting surgical outcomes. Cornea 24, S2–s11. [PubMed: 16227819]

Fukuto A, Kim S, Kang J, Gates BL, Chang MW, Pinkerton KE, Van Winkle LS, Kiuchi Y, Murphy CJ, Leonard BC, Thomasy SM, 2021. Metal oxide engineered nanomaterials modulate rabbit corneal fibroblast to myofibroblast transformation. Transl. Vis. Sci. Technol 10, 23.

Giulio MD, Zappacosta R, Lodovico SD, Campli ED, Siani G, Fontana A, Cellini L, 2018. Antimicrobial and antibiofilm efficacy of graphene oxide against chronic wound microorganisms. Antimicrob. Agents Chemother 62, e00547, 00518. [PubMed: 29661876]

Hemmer MJ, Barron MG, Greene RM, 2011. Comparative toxicity of eight oil dispersants, Louisiana sweet crude oil (LSC), and chemically dispersed LSC to two aquatic test species. Environ. Toxicol. Chem 30, 2244–2252. [PubMed: 21766318]

Herner JD, Green PG, Kleeman MJ, 2006. Measuring the trace elemental composition of size-resolved airborne particles. Environ. Sci. Technol 40, 1925–1933. [PubMed: 16570617]

Huang C, Zhang X, Li Y, Yang X, 2021. Hyaluronic acid and graphene oxide loaded silicon contact lens for corneal epithelial healing. J. Biomater. Sci. Polym. Ed 32, 372–384. [PubMed: 33058750]

Huang J-F, Zhong J, Chen G-P, Lin Z-T, Deng Y, Liu Y-L, Cao P-Y, Wang B, Wei Y, Wu T, Yuan J, Jiang G-B, 2016. A hydrogel-based hybrid theranostic contact lens for fungal keratitis. ACS Nano 10, 6464–6473. [PubMed: 27244244]

Jester JV, Huang J, Barry-Lane PA, Kao WW, Petroll WM, Cavanagh HD, 1999. Transforming growth factor(beta)-mediated corneal myofibroblast differentiation requires actin and fibronectin assembly. Invest. Ophthalmol. Vis. Sci 40, 1959–1967. [PubMed: 10440249]

Jester JV, Petroll WM, Barry PA, Cavanagh HD, 1995. Expression of alpha-smooth muscle (alpha-SM) actin during corneal stromal wound healing. Invest. Ophthalmol. Vis. Sci 36, 809–819. [PubMed: 7706029]

Jiang T, Amadei CA, Lin Y, Gou N, Rahman SM, Lan J, Vecitis CD, Gu AZ, 2021. Dependence of graphene oxide (GO) toxicity on oxidation level, elemental composition, and size. Int. J. Mol. Sci 22.

Kan Z, Zhao KX, Jiang C, Liu DY, Guo Y, Liu LY, Wang WJ, He ZQ, Zhang ZF, Wang SY, 2022. Respiratory exposure to graphene oxide induces pulmonary fibrosis and organ damages in rats involving caspase-1/p38MAPK/TGF-β1 signaling pathways. Chemosphere 303, 135181. [PubMed: 35667501]

Kim S, Gates BL, Chang M, Pinkerton KE, Van Winkle L, Murphy CJ, Leonard BC, Demokritou P, Thomasy SM, 2021. Transcorneal delivery of topically applied silver nanoparticles does not delay epithelial wound healing. NanoImpact 24.

Kim S, Gates BL, Leonard BC, Gragg MM, Pinkerton KE, Van Winkle LS, Murphy CJ, Pyrgiotakis G, Zhang Z, Demokritou P, Thomasy SM, 2020. Engineered metal oxide nanomaterials inhibit corneal epithelial wound healing in vitro and in vivo. NanoImpact 17.

Lammel T, Boisseaux P, Fernández-Cruz M-L, Navas JM, 2013. Internalization and cytotoxicity of graphene oxide and carboxyl graphene nanoplatelets in the human hepatocellular carcinoma cell line Hep G2. Part. Fibre Toxicol 10, 27. [PubMed: 23849434]

Lee JH, Park SJ, Choi JW, 2019. Electrical property of graphene and its application to electrochemical biosensing. Nanomaterials 9.

Lee S, Jo I, Kang S, Jang B, Moon J, Park JB, Lee S, Rho S, Kim Y, Hong BH, 2017. Smart contact lenses with graphene coating for electromagnetic interference shielding and dehydration protection. ACS Nano 11, 5318–5324. [PubMed: 28199121]

Liao KH, Lin YS, Macosko CW, Haynes CL, 2011. Cytotoxicity of graphene oxide and graphene in human erythrocytes and skin fibroblasts. ACS Appl. Mater. Interfaces 3, 2607–2615. [PubMed: 21650218]

Liao Y, Wang W, Huang X, Sun Y, Tian S, Cai P, 2018. Reduced graphene oxide triggered epithelial-mesenchymal transition in A549 cells. Sci. Rep 8, 15188. [PubMed: 30315228]

Ljubimov AV, Saghizadeh M, 2015. Progress in corneal wound healing. Prog. Retin. Eye Res 49, 17–45. [PubMed: 26197361]

Mohammed H, Kumar A, Bekyarova E, Al-Hadeethi Y, Zhang X, Chen M, Ansari MS, Cochis A, Rimondini L, 2020. Antimicrobial mechanisms and effectiveness of graphene and graphene-functionalized biomaterials. A scope review. Front. Bioeng. Biotechnol 8, 465. [PubMed: 32523939]

Myrna KE, Mendonsa R, Russell P, Pot SA, Liliensiek SJ, Jester JV, Nealey PF, Brown D, Murphy CJ, 2012. Substratum topography modulates corneal fibroblast to myofibroblast transformation. Invest. Ophthalmol. Vis. Sci 53, 811–816. [PubMed: 22232431]

Nasirzadeh N, Azari MR, Rasoulzadeh Y, Mohammadian Y, 2019. An assessment of the cytotoxic effects of graphene nanoparticles on the epithelial cells of the human lung. Toxicol. Ind. Health 35, 79–87. [PubMed: 30803420]

Ou L, Lv X, Wu Z, Xia W, Huang Y, Chen L, Sun W, Qi Y, Yang M, Qi L, 2021. Oxygen content-related DNA damage of graphene oxide on human retinal pigment epithelium cells. J. Mater. Sci. Mater. Med 32, 20. [PubMed: 33638700]

Park EJ, Lee GH, Han BS, Lee BS, Lee S, Cho MH, Kim JH, Kim DW, 2015. Toxic response of graphene nanoplatelets in vivo and in vitro. Arch. Toxicol 89, 1557–1568. [PubMed: 24980260]

Parviz D, Strano M, 2018. Endotoxin-free preparation of graphene oxide and graphene-based materials for biological applications. Curr. Protoc. Chem.Biol 10, e51. [PubMed: 30285316]

Pelin M, Fusco L, Martin C, Sosa S, Frontinan-Rubio J, Gonzalez-Dominguez JM, Duran-Prado M, Vazquez E, Prato M, Tubaro A, 2018. Graphene and graphene oxide induce ROS production in human HaCaT skin keratinocytes: the role of xanthine oxidase and NADH dehydrogenase. Nanoscale 10, 11820–11830. [PubMed: 29920573]

Perreault F, Fonseca de Faria A, Elimelech M, 2015. Environmental applications of graphene-based nanomaterials. Chem. Soc. Rev 44, 5861–5896. [PubMed: 25812036]

Robertson DM, Li L, Fisher S, Pearce VP, Shay JW, Wright WE, Cavanagh HD, Jester JV, 2005. Characterization of growth and differentiation in a telomerase-immortalized human corneal epithelial cell line. Invest. Ophthalmol. Vis. Sci 46, 470–478. [PubMed: 15671271]

Seabra AB, Paula AJ, De Lima R, Alves OL, Duŕan N, 2014. Nanotoxicity of graphene and graphene oxide. Chem. Res. Toxicol 27, 159–168. [PubMed: 24422439]

Tian X, Yang Z, Duan G, Wu A, Gu Z, Zhang L, Chen C, Chai Z, Ge C, Zhou R, 2017. Graphene oxide nanosheets retard cellular migration via disruption of actin cytoskeleton. Small 13.

Wang A, Pu K, Dong B, Liu Y, Zhang L, Zhang Z, Duan W, Zhu Y, 2013. Role of surface charge and oxidative stress in cytotoxicity and genotoxicity of graphene oxide towards human lung fibroblast cells. J. Appl. Toxicol 33, 1156–1164. [PubMed: 23775274]

Wilson SE, 2020. Corneal myofibroblasts and fibrosis. Exp. Eye Res 201, 108272. [PubMed: 33010289]

Wu W, Yan L, Wu Q, Li Y, Li Q, Chen S, Yang Y, Gu Z, Xu H, Yin ZQ, 2016. Evaluation of the toxicity of graphene oxide exposure to the eye. Nanotoxicology 10, 1329–1340. [PubMed: 27385068]

Yang HW, Hua MY, Chen SL, Tsai RY, 2013. Reusable sensor based on high magnetization carboxyl-modified graphene oxide with intrinsic hydrogen peroxide catalytic activity for hydrogen peroxide and glucose detection. Biosens. Bioelectron 41, 172–179. [PubMed: 22959012]

Zahin N, Anwar R, Tewari D, Kabir MT, Sajid A, Mathew B, Uddin MS, Aleya L, Abdel-Daim MM, 2020. Nanoparticles and its biomedical applications in health and diseases: special focus on drug delivery. Environ. Sci. Pollut. Res. Int 27, 19151–19168. [PubMed: 31079299]

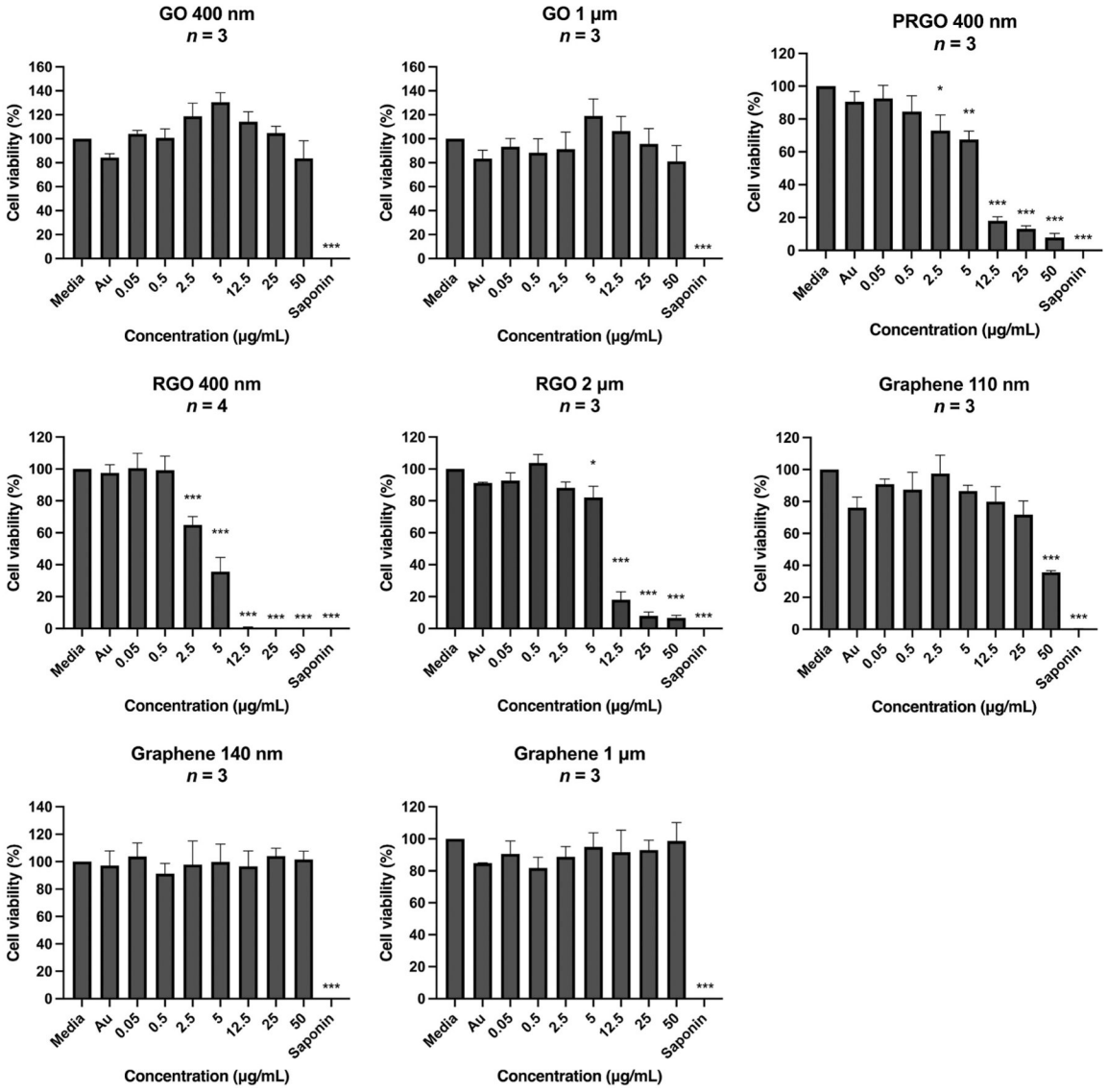

Fig. 1.

Effect of eight GBNs on hTCEpi cell viability as measured by Calcein AM assay. Data are represented as mean ± standard error of the mean (SEM). Error bars represent the SEM and asterisks indicate significant differences using a one-way ANOVA followed by Dunnett's multiple comparisons test compared to the media controls at $*P < 0.05$, $**P < 0.01$, $***P < 0.001$. The number of independent experiments (n) which included six technical replicates is designated in the figure.

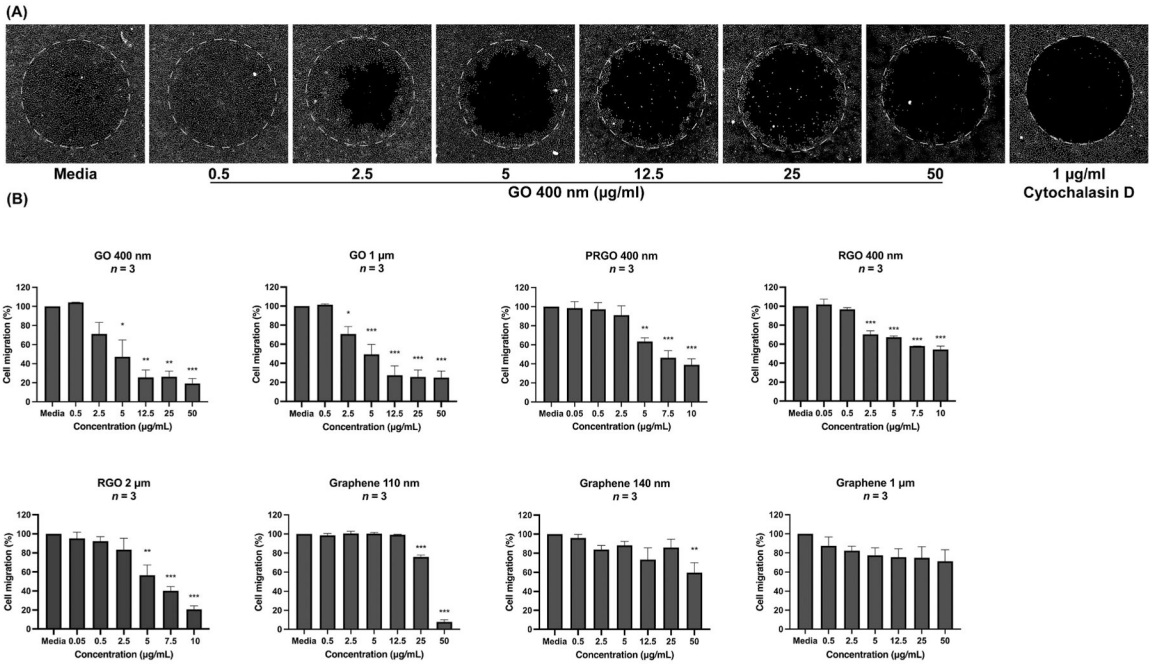

Fig. 2.

Effect of eight GBNs on hTCEpi cell migration as measured by round wound healing assay. (A) Representative images of migration assay of hTCEpi cells treated with 0.5–50 μg/ml of GO (400 nm). (B) The data represent mean ± standard error of the mean (SEM). Error bars represent the SEM and asterisks indicate significant differences identified with a one-way ANOVA followed by Dunnett's multiple comparisons test when compared to the media controls; $*P < 0.05$, $**P < 0.01$, $***P < 0.001$. The number of independent experiments (n) with three technical replicates is denoted in the figure.

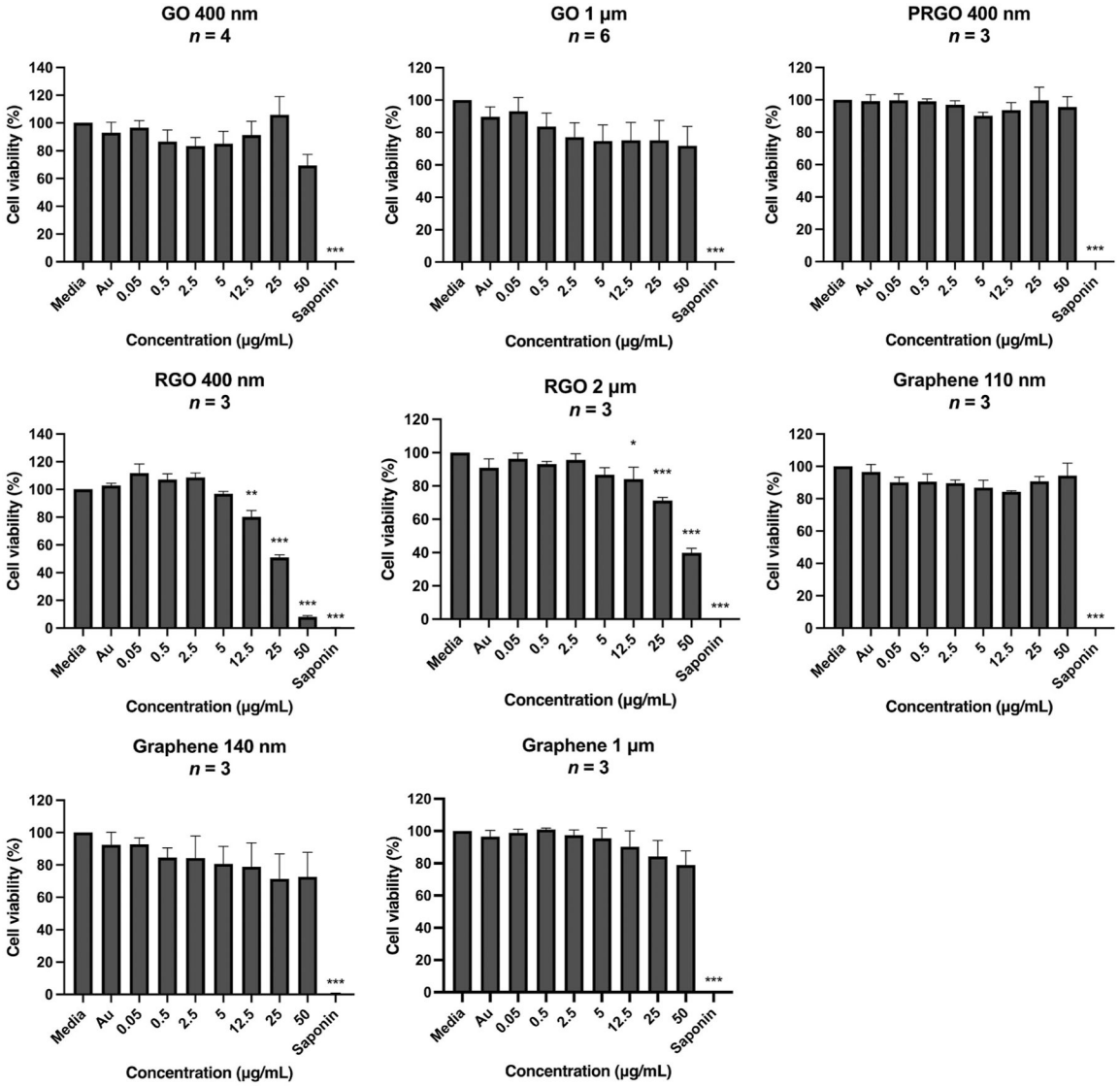

Fig. 3.

Effect of eight GBNs on RCF viability as measured by Calcein AM assay. Data are represented as mean ± standard error of the mean (SEM) with error bars denoting SEM. Asterisks indicate significant differences compared to the media controls at $*P < 0.05$, $**P < 0.01$, $***P < 0.001$ using a one-way ANOVA followed by Dunnett's multiple comparisons test. The number of independent experiments (n) with six technical replicates is designated in the figure.

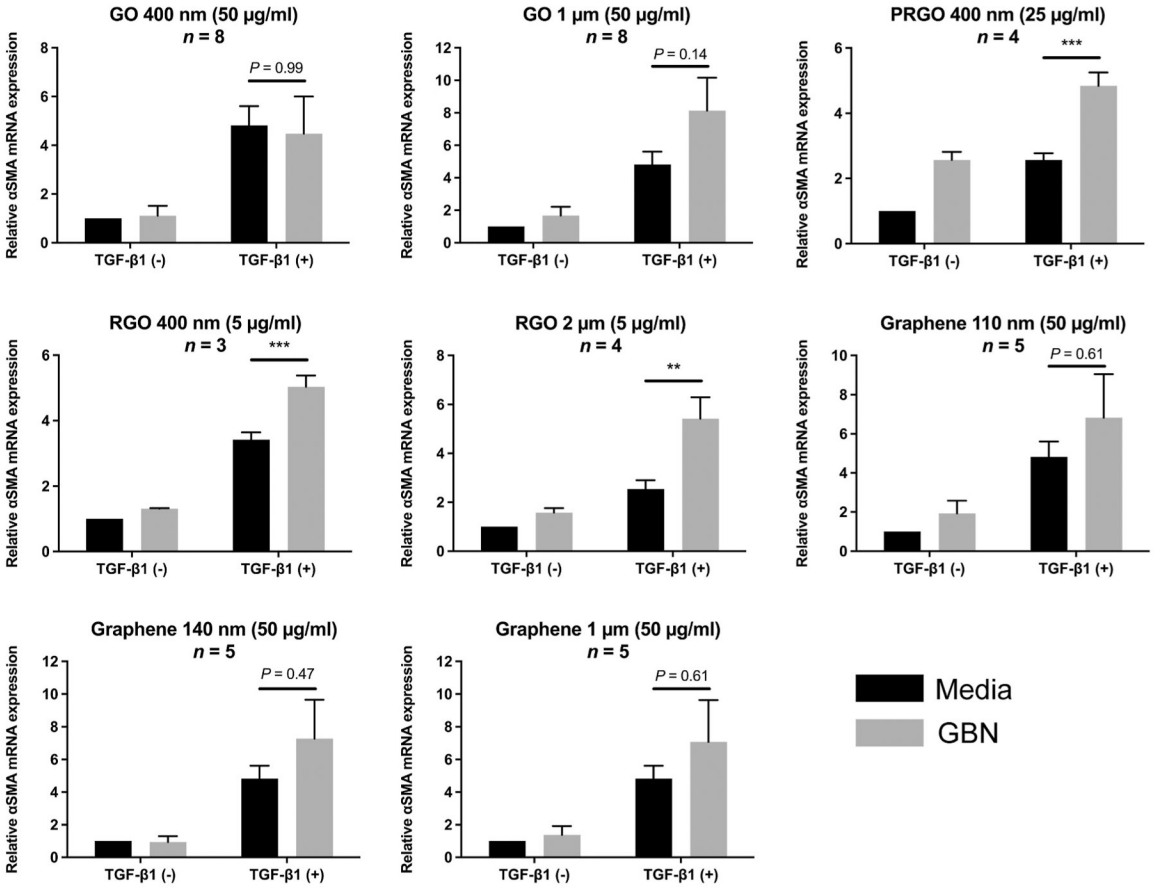

Fig. 4.

Gene expression of αSMA after 24-h treatment of RCFs with GBNs analyzed by quantitative real-time PCR. The results were expressed as $2^{-\Delta\Delta CT}$ with GAPDH used as the endogenous control. Data are mean ± standard error of the mean (SEM) with error bars indicating SEM; $^{**}P < 0.01$, $^{***}P < 0.001$, one-way ANOVA followed by Tukey's multiple comparisons test was performed to compare with TGF-β1 treatment only. The number of independent experiments (*n*) with three technical replicates is denoted in the figure.

Table 1

General characteristics of the eight graphene-based nanomaterials.

Nanomaterial name (Serial number)	Particle size	Dispersant	Dispersion concentration	Synthesis method
Graphene oxide (GO-400NMX400NM-DP20190115-1)	400 nm	Water	310 μg/ml	Improved Hummer's method and liquid-phase exfoliation
Graphene oxide (GO-1μMX1μM-DP20190115-1)	1 μm	Water	500 μg/ml	Improved Hummer's method and liquid-phase exfoliation
Partially reduced graphene oxide (PRGO-400NMX400NM-DP20190630-1)	400 nm	Sodium cholate (4 mg/ml)	500 μg/ml	Improved Hummer's method and liquid-phase exfoliation
Reduced graphene oxide (RGO-400NMx400NM-DP04302018-1)	400 nm	Sodium cholate (3.88 mg/ml)	500 μg/ml	Modified Hummer's method and liquid-phase exfoliation
Reduced graphene oxide (rGO-2μMX2μM-DP20190220-1)	2 μm	Sodium cholate (2.5 mg/ml)	400 μg/ml	Improved Hummer's method and liquid-phase exfoliation
Graphene (G-110NMX110NM-DP20170315-1)	110 nm	Sodium cholate (5 mg/ml)	500 μg/ml	Liquid-phase exfoliation
Graphene (G-PF108-140NMX140NM-DP20190801-1)	140 nm	Pluronic® F-108 (10 mg/ml)	320 μg/ml	Liquid-phase exfoliation
Graphene (G-PF108-1μMX1μM-DP20190801-1)	1 μm	Pluronic® F-108 (10 mg/ml)	320 μg/ml	Liquid-phase exfoliation